Original Article

Preoperative assessment of Ki-67 expression in hepatocellular carcinoma using a multi-parametric spectral CT approach

Jinling Deng[#], Qin Tang[#], Qijun Wei, Fengqiu Ruan, Xuan Li, Liling Long

Department of Radiology, the First Affiliated Hospital of Guangxi Medical University, Nanning, China

Contributions: (I) Conception and design: J Deng, L Long; (II) Administrative support: L Long; (III) Provision of study materials or patients: Q Tang, Q Wei; (IV) Collection and assembly of data: J Deng, Q Tang; (V) Data analysis and interpretation: J Deng, F Ruan, X Li; (VI) Manuscript writing: All authors; (VII) Final approval of manuscript: All authors.

[#]These authors contributed equally to this work.

Correspondence to: Liling Long, PhD, MD. Department of Radiology, the First Affiliated Hospital of Guangxi Medical University, 6 Shuangyong Road, Nanning 530021, China. Email: cjr.longliling@vip.163.com.

Background: Ki-67 is a pivotal biomarker for evaluating the prognosis of hepatocellular carcinoma (HCC). This study aimed to investigate the utility of qualitative and quantitative parameters derived from spectral computed tomography (CT) in assessing Ki-67 expression in HCC.

Methods: This prospective, single-center study included 89 patients (94 lesions) with pathologically confirmed HCC from February 2023 to February 2024. Participants underwent enhanced abdominal spectral CT scans within one week prior to surgery. The patients were divided into the following two groups based on the positive rate of Ki-67 (Ki-67%): a high-expression group (Ki-67 >20%, n=42); and a low-expression group (Ki-67 ≤20%, n=52). The spectral parameters assessed included CT values at 40 and 70 keV, iodine concentration (IC), the slope of the spectral Hounsfield unit (HU) curve (λHU), normalized iodine concentration (NIC) during the arterial phase (AP) and portal venous phase (PVP), and extracellular volume (ECV) fraction. Statistical significance of spectral CT parameters related to Ki-67 expression status was compared across different groups, and correlations between spectral CT parameters and Ki-67 expression levels were analyzed.

Results: Significant differences were observed between the low and high Ki-67 expression groups concerning age, alpha-fetoprotein (AFP) levels, and capsule integrity (P=0.002, P=0.013, and P=0.005, respectively). Notable differences were also found in intratumoral NIC-AP, NIC-PVP, AP slope, PVP slope, and ECV fraction (P=0.017, P=0.005, P=0.001, P<0.001, and P=0.001, respectively). Meanwhile, in the comparative analysis between the low and high expression group of Ki-67, there were no statistically significant differences in the peritumoral <1 cm NIC-AP and NIC-PVP, as well as transtumoral NIC-AP and NIC-PVP levels (P>0.05). Ki-67 expression in HCC exhibited negative correlations with intratumoral NIC-AP (r=–0.248; P=0.016), NIC-PVP (r=–0.291; P=0.004), AP slope (r=–0.330; P=0.001), PVP slope (r=–0.367; P<0.001), and ECV fraction (r=–0.339; P=0.001).

Conclusions: Qualitative and quantitative parameters from spectral CT provide valuable information for distinguishing between low and high Ki-67 expression in HCC.

Keywords: Spectral computed tomography (spectral CT); hepatocellular carcinoma (HCC); Ki-67 index; quantitative parameters; peritumoral

Submitted Oct 23, 2024. Accepted for publication Feb 28, 2025. Published online Apr 27, 2025.
doi: 10.21037/qims-24-2313
View this article at: https://dx.doi.org/10.21037/qims-24-2313

Introduction

Hepatocellular carcinoma (HCC) represented the sixth most common cancer and the third leading cause of cancer-related deaths worldwide in 2022 (1). The 5-year survival rate for HCC is approximately 18% (2,3), with a median overall survival of only 20–30 months (4). A significant factor contributing to this poor prognosis is the high recurrence rate following curative liver resection, which has been reported to exceed 70% within 5 years (3,5).

Ki-67 is a biomarker for cell proliferation and is associated with the prognosis of malignant tumors. The Ki-67 proliferation index reflects the level of proliferative activity and demonstrates a significant correlation with tumor grading (6). In HCC, Ki-67 expression serves as an independent prognostic indicator for disease-free survival and overall survival (7). High Ki-67 expression is a significant risk factor contributing to the elevated recurrence rate and poor prognosis following curative resection of HCC (8,9). Unfortunately, Ki-67 assessment is typically performed pathologically, necessitating careful identification across multiple regions of resected specimens. Thus, accurate preoperative detection of Ki-67 status in HCC patients could provide critical clinical insights to improve survival rates and outcomes.

Compared to conventional computed tomography (CT), spectral CT offers multi-parametric imaging, quantitative analysis, and spectral evaluation (10). Previous studies have indicated that quantitative parameters from spectral CT can predict Ki-67 expression in lung, breast, and colorectal cancers (11-14). However, there are limited reports on the correlation between spectral CT and Ki-67 expression in liver cancer, with only two studies demonstrating a positive correlation between the quantitative parameters of intratumoral tissue and Ki-67 levels (15,16). Furthermore, recurrence or metastasis of liver cancer predominantly occurs within the liver, highlighting the significant role of peritumoral tissues in the dissemination of cancer cells (17), which is crucial for prognostic prediction (18). Nevertheless, no studies have evaluated the qualitative and quantitative parameters of spectral CT in both intratumoral and peritumoral regions to predict Ki-67 expression in HCC. Thus, the objective of this study was to determine whether assessments based on spectral CT imaging of intratumoral and peritumoral regions can yield valuable insights into Ki-67 expression status in liver cancer. We present this article in accordance with the STROBE reporting checklist (available at https://qims.amegroups.com/article/view/10.21037/qims-24-2313/rc).

Methods

Patients

This study was conducted in accordance with the Declaration of Helsinki and its subsequent amendments. This prospective study was approved by the Medical Ethics Committee of the First Affiliated Hospital of Guangxi Medical University (approval No. 2024-E691-01) and written informed consent was provided by all patients prior to participation. Between February 2023 and February 2024, a total of 163 patients with suspected HCC based on ultrasound or magnetic resonance imaging (MRI) underwent preoperative spectral CT imaging. The inclusion criteria were as follows: (I) pathologically confirmed primary HCC; (II) spectral CT examination within one week prior to surgery; and (III) availability of complete clinical and imaging data. The exclusion criteria were as follows: (I) preoperative anticancer treatment; and (II) images that failed to meet quality control standards. The patient selection flowchart for the study is shown in *Figure 1*.

Ki-67 assessment

The Ki-67 proliferation index was determined by two pathologists (with 5 and 15 years of experience, respectively) using high-power microscopy (×400). They randomly selected 10 fields on each slide and recorded a total of 1,000 cells. The percentage of positively stained Ki-67 nuclei was calculated semi-quantitatively. The Ki-67 index was initially assessed by the junior physician and ultimately determined by the senior physician. The Ki-67 index was defined as the percentage of Ki-67-positive nuclei. Based on the median Ki-67 expression index in this study, patients were classified into two groups: a high Ki-67 expression group (more than 20% positive cells) and a low Ki-67 expression group (20% or fewer positive cells).

Spectral CT protocol

All examinations were conducted using a GE Revolution CT scanner (GE Healthcare, Chicago, IL, USA), with patients positioned supine and head-first. A conventional non-contrast scan of the upper abdomen was performed at a tube voltage of 120 kV, with automatic selection of tube current, covering from the diaphragm to the lower poles of the kidneys. A high-pressure injector administered the contrast medium via the antecubital vein, at a dosage of 1.5 mL/kg body weight at a rate of 4.5 mL/s, followed by a

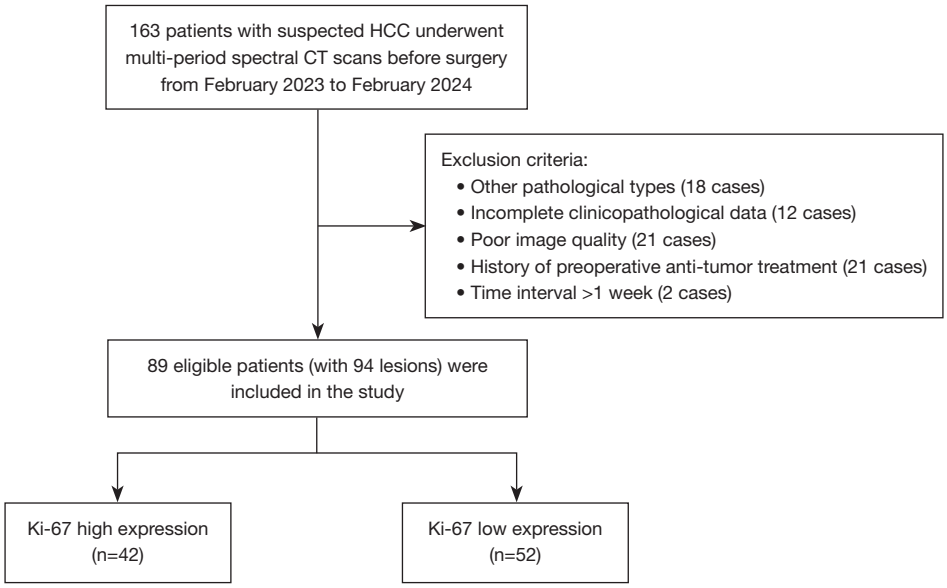

Figure 1 Flowchart illustrating the patient selection process in this study. CT, computed tomography; HCC, hepatocellular carcinoma.

30-mL saline flush at the same rate. Three-phase spectral enhanced scans were conducted approximately at 33, 65, and 127 seconds post-contrast injection to obtain arterial, portal venous, and delayed phase images, respectively. Gemstone spectral imaging (GSI) utilized spiral scanning with instantaneous switching between 80 and 140 kVp, with tube current automatically selected by GSI Assist and 60% adaptive statistical iterative reconstruction-V (ASiR-V). Image reconstruction involved combining the non-contrast and three-phase spectral enhanced data with 50% ASIR-V, resulting in a slice thickness and interval of 1.25 mm.

Image analysis and data collection

Using the spectral reconstruction algorithm on an Advantage Windows server (version 4.7, GE Medical Systems), images of 40 keV virtual monochromatic imaging (VMI), 70 keV VMI, and iodine concentration map (IC Map) were generated. Two radiologists (a senior physician and a junior physician) independently analyzed the spectral CT images of 42 lesions, blinded to clinical and pathological data. Thereafter, the junior radiologist delineated the remaining 52 lesions.

Initially, tumor margins were identified on the 70 keV VMI images from the arterial (AP) and portal venous phase (PVP). Regions of interest (ROIs) with a diameter of 8 mm were manually outlined as follows: (I) tumor: three ROIs were delineated in the solid portion of the tumor, avoiding vascular areas, necrotic regions, and tumor edges, based on the maximum diameter; if the short diameter of the solid portion was less than 8 mm, the largest possible ROI was selected; (II) peritumoral: draw three ROIs within 10 mm of the tumor margin; draw three ROIs across the tumor margin (with approximately half inside and half outside the tumor); (III) abdominal aorta: an ROI was drawn at the same slice level as the lesion, avoiding vessel edges and calcifications. The ROIs were then copied to the corresponding slices of other spectral parameter images (40 keV VMI, 70 keV VMI, and IC Map) to measure the respective values.

During the equilibrium phase, ROIs were delineated solely on the IC Map: (I) tumor: three ROIs were placed within the solid portion of the tumor, avoiding areas of necrosis; (II) abdominal aorta: one ROI was delineated on the abdominal aorta at the same slice level as the lesion, avoiding the vessel margins and calcifications (*Figure 2*).

The normalized iodine concentration (NIC) for both AP and PVP was calculated using the formula: NIC = IC lesion/IC abdominal aorta. Additionally, the slope of the spectral curve (λHU) was calculated using: λHU = (CT40 keV – CT70 keV)/(70 keV – 40 keV), representing the difference in CT values at two energy levels divided by the energy difference. The extracellular volume (ECV) fraction was computed as follows: ECV = (1 – hematocrit) × (iodine concentration of the lesion during the equilibrium phase/iodine concentration of the abdominal aorta at the same level during the equilibrium phase).

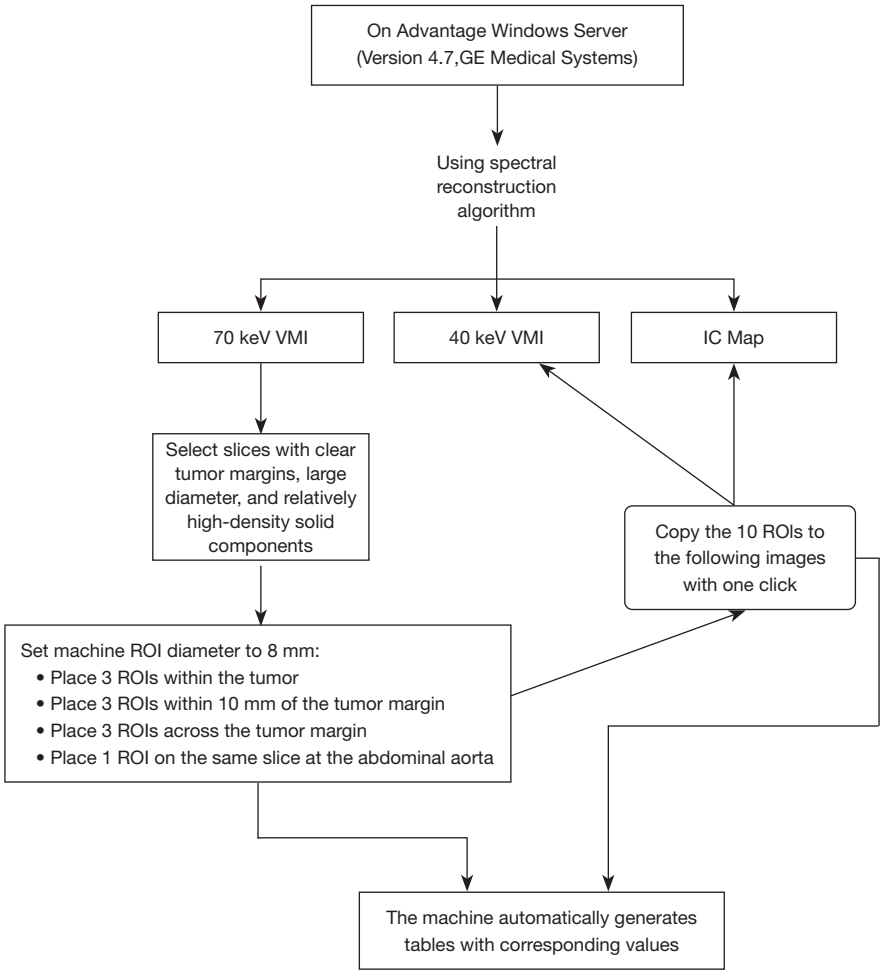

Figure 2 Flowchart for region of interest delineation in arterial and portal venous phase. IC Map, iodine concentration map; ROI, region of interest; VMI, virtual monochromatic imaging.

Quality control of ROI delineation

In the 70 keV VMI mode, the liver is initially evaluated to identify slices where tumor margins are clearly delineated and there is adequate surrounding tissue for ROI placement. The selected slices should also contain relatively high-density solid components within the tumor and exhibit the largest possible diameter. If delineating tumor margins proves challenging in the 70 keV VMI, the IC map can be consulted. Should it still be difficult to identify a suitable slice that meets these criteria, a senior radiologist will be consulted to determine the appropriate slice or exclude the patient from the study. The system is configured to generate ROIs with a diameter of 8 mm. During ROI placement, care must be taken to avoid vascular regions, areas of tumor necrosis, and calcifications. Since the 40 keV VMI, 70 keV VMI, and IC map are displayed simultaneously, the 10 ROIs identified in the 70 keV VMI can be readily copied to corresponding slices in the other two images with a single click. If the measured data between the two observers show significant discrepancies, the ROIs will be redrawn. When delineating ROIs on PVP images, the placement of the 10 ROIs should be as similar as possible to their counterparts in the AP. This allows for verification of the correctness of the AP ROIs outlined in the previous step. Should any discrepancies be identified, the AP ROIs should be redrawn (*Figure 3*).

Statistical analysis

Statistical analyses were conducted using the software SPSS 23.0 (IBM Corp., Armonk, NY, USA). The reliability of the

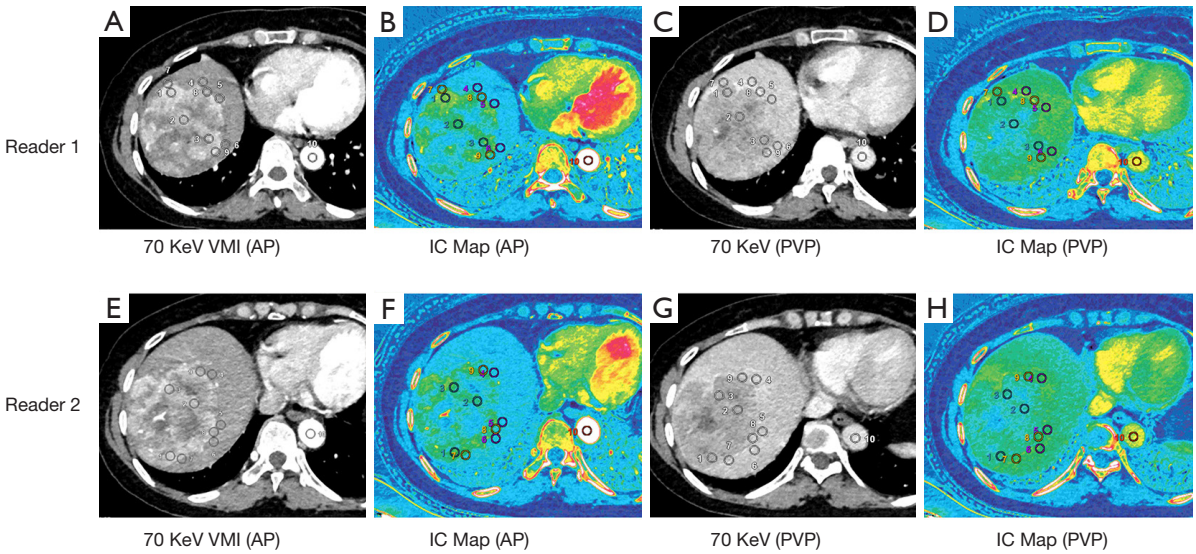

Figure 3 Imaging examination of a 54-year-old female patient with a 9.1-cm single hepatocellular carcinoma. ROI123 outlines the solid part within the tumor, ROI456 is within 10 mm of the tumor margin, ROI789 spans across the tumor margin, and ROI10 delineates the abdominal aorta at the same level. The first row (A-D) represents the delineations by Reader 1, whereas the second row (E-H) represents those by Reader 2. (A,E) Arterial phase 70-keV VMI; (B,F) arterial phase iodine maps, showing intratumoral NIC-AP of 0.22 and 0.18, peritumoral NIC-AP (<1 cm) of 0.09 and 0.09, and transtumoral NIC-AP of 0.15 and 0.14, respectively; (C,G) portal venous phase 70-keV VMI; (D,H) portal venous phase iodine maps, showing intratumoral NIC-PVP of 0.50 and 0.49, peritumoral NIC-PVP (<1 cm) of 0.67 and 0.65, and transtumoral NIC-PVP of 0.64 and 0.63, respectively. AP, arterial phase; IC Map, iodine concentration map; NIC, normalized iodine concentration; ROI, region of interest; VMI, virtual monochromatic imaging; PVP, portal venous phase.

spectral parameter assessments of 42 lesions by two observers was measured using the intraclass correlation coefficient (ICC) and Bland-Altman analysis. Clinical and imaging data from patients meeting the inclusion and exclusion criteria were collected, and differences in spectral CT parameters among groups based on Ki-67 expression levels were analyzed. Both Pearson and Spearman correlation analyses were employed to assess the relationship between spectral CT parameters and Ki-67 indices.

Results

In this study, a total of 163 patients underwent scanning. Cases were excluded based on the following criteria: 18 cases with postoperative pathology indicating non-HCC, 12 cases with incomplete clinical and pathological data, 21 cases with poor image quality, 21 cases with a history of preoperative antitumor treatment, and 2 cases where the scanning time was more than one week apart from surgery. This resulted in a final cohort of 89 patients, encompassing 94 lesions.

Patient clinical characteristics

A total of 94 eligible lesions were included in this study. The clinical characteristics of the participants are summarized in *Table 1*. Significant differences were observed between the low and high Ki-67 expression groups in terms of age and alpha-fetoprotein (AFP) levels (P<0.05).

Inter-observer consistency of quantitative parameters

The measurements of spectral CT quantitative parameters demonstrated good inter-observer consistency, with an ICC >0.8 (*Table 2*). Furthermore, Bland-Altman analysis was conducted, with the majority of data points falling between +1.96 standard deviation (SD) and –1.96 SD (*Figure 4*).

Value of spectral CT imaging features in evaluating Ki-67 expression

Imaging features of HCC assessed by CT included tumor size, presence of cirrhosis, number of tumors, tumor margins, peritumoral enhancement in the AP, capsule

Table 1 Comparison of preoperative patient characteristics

Variables	Ki-67 low expression (n=52)	Ki-67 high expression (n=42)	P value
Age (years)[†]	57.81±11.10	51.19±8.60	0.002
Sex			0.635
Men	40 (76.9)	34 (81.0)	
Women	12 (23.1)	8 (19.0)	
AFP (ng/mL)[‡]	9.41 (3.04, 134.06)	83.54 (6.25, 3,626.00)	0.013
PIVKA-II (mAU/mg)[‡]	112.02 (48.50, 1,020.70)	328.44 (38.81, 2,516.88)	0.429

Data are numbers of lesions, with percentages in parentheses. Categorical variables were compared by using the χ^2 test or Fisher exact test. [†], data are mean ± standard deviation and compared by using the two-sample *t*-test; [‡], data are medians, with interquartile ranges in parentheses and compared by using the Mann-Whitney *U* test. AFP, alpha-fetoprotein; PIVKA-II, Protein Induced by Vitamin K Absence or Antagonist-II.

Table 2 Evaluation on the consistency of spectral parameters measured by two observers

CT parameter	ICC	95% CI	P value
Intratumoral NIC-AP	0.905	0.824–0.948	<0.001
Intratumoral NIC-PVP	0.941	0.885–0.969	<0.001
Peritumoral <1 cm NIC-AP	0.955	0.909–0.977	<0.001
Peritumoral <1 cm NIC-PVP	0.884	0.795–0.936	<0.001
Transtumoral NIC-AP	0.927	0.869–0.960	<0.001
Transtumoral NIC-PVP	0.920	0.856–0.956	<0.001
λHU-AP	0.942	0.895–0.968	<0.001
λHU-PVP	0.957	0.915–0.978	<0.001
ECV	0.892	0.728–0.950	<0.001

AP, arterial phase; CI, confidence interval; CT, computed tomography; ECV, extracellular volume; ICC, intraclass correlation coefficient; NIC, normalized iodine concentration; PVP, portal venous phase; λHU, slope of the spectral Hounsfield unit curve.

integrity, and large vessel invasion. Notably, a significant difference in capsule integrity was observed between the low and high Ki-67 expression groups (P<0.05) (*Table 3*).

Value of spectral CT quantitative parameters in evaluating Ki-67 expression

Significant differences were observed between the low and high Ki-67 expression groups regarding intratumoral NIC during the arterial phase (NIC-AP), intratumoral NIC during the portal venous phase (NIC-PVP), AP slope, PVP slope, and ECV fraction (P<0.05) (*Table 4*). Additionally, Ki-67 expression in HCC exhibited negative correlations with intratumoral NIC-AP, intratumoral NIC-PVP, AP slope, PVP slope, and ECV (P<0.05), as detailed in *Table 5*.

Discussion

In this study, patients within the high Ki-67 expression group were generally younger, exhibited higher AFP levels, and presented with incomplete or absent capsules. These findings are consistent with the observations made by Wu *et al.* (19) and Xu *et al.* (15). Elevated AFP levels and incomplete capsules have been associated with increased invasiveness in HCC (20,21).

Among the quantitative parameters derived from spectral CT, significant differences were observed between the low and high Ki-67 expression groups in intratumoral NIC-AP, NIC-PVP, AP slope, PVP slope, and ECV, all of which demonstrated negative correlations.

Regarding the slopes, these findings align with the results from Chen *et al.* (14) and Wang *et al.* (22), suggesting that

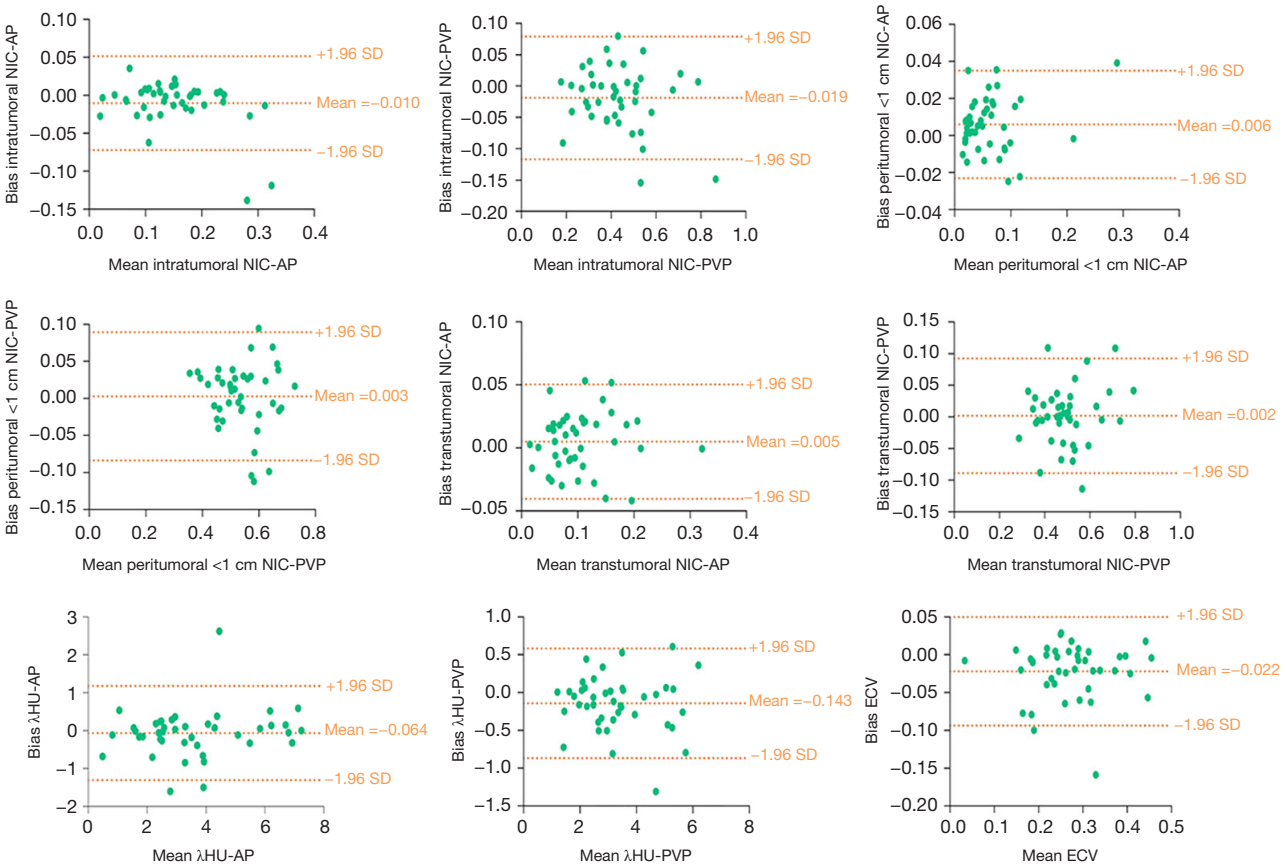

Figure 4 Bland-Altman analysis of the measurement data by two radiologists. AP, arterial phase; ECV, extracellular volume; NIC, normalized iodine concentration; SD, standard deviation; PVP, portal venous phase; λHU, slope of the spectral Hounsfield unit curve.

variations in the chemical molecular structures of different substances result in distinct energy attenuation curves (23). This underscores the significant correlation observed between Ki-67 expression and slopes in HCC.

Intratumoral NIC-AP and NIC-PVP also serve to differentiate Ki-67 expression status, aligning with the findings of Xu *et al.* (15), which suggest that standardized ICs may reflect Ki-67 levels. Iodine maps can provide preliminary evaluations of tumor blood supply and hemodynamics based on ICs (24).

Meanwhile, Xu *et al.* (15) reported a positive correlation between intratumoral NIC-AP, NIC-PVP, and Ki-67, which contrasts with our findings. Emerging evidence suggests that in HCC, a high tumor proliferation rate is frequently associated with the development of a hypoxic microenvironment (25). Although hypoxia induces the expression of pro-angiogenic factors such as erythropoietin and vascular endothelial growth factor (VEGF), the resulting angiogenesis is often compromised by disorganized endothelial cell alignment, leading to the formation of non-functional or abnormal vessels (26). Furthermore, the rapid proliferation of cancer cells generates significant solid stress, which can compress intratumoral blood vessels and subsequently impair blood flow (27). Consequently, high Ki-67 expression, a marker of robust cell proliferation, may paradoxically result in reduced intratumoral blood supply.

Additionally, we hypothesize that this phenomenon may be associated with the placement of the ROI. In our study, establishing a one-to-one correspondence between the ROIs delineated on CT images and those on histopathological sections posed significant challenges. Prior research has suggested that in poorly differentiated HCC, the hepatic cancer tissue surrounding the tumor may necessitate an increased blood supply due to its invasive proliferative characteristics (28,29), leading to relatively higher ICs.

Regarding ECV, Wang *et al.* (30) showed a positive

Table 3 Comparison of preoperative imaging characteristics of patients

Parameter	Ki-67 low expression (n=52)	Ki-67 high expression (n=42)	P value
Tumor size (cm)†	3.80 (2.75, 5.38)	3.60 (2.50, 7.03)	0.831
Liver cirrhosis			0.137
No	17 (32.7)	8 (19.0)	
Yes	35 (67.3)	34 (81.0)	
Number of nodules			0.748
1	42 (80.8)	35 (83.3)	
≥2	10 (19.2)	7 (16.7)	
Boundary			0.344
Clear	17 (32.7)	10 (23.8)	
Vague	35 (67.3)	32 (76.2)	
Leafing			0.132
No	34 (65.4)	21 (50.0)	
Yes	18 (34.6)	21 (50.0)	
Perianeurysmal enhancement in the arterial phase			>0.99
No	48 (92.3)	38 (90.5)	
Yes	4 (7.7)	4 (9.5)	
False envelope			0.005
Complete	30 (57.7)	12 (28.6)	
None or incomplete	22 (42.3)	30 (71.4)	
Invasion of large vessels			0.073
No	50 (96.2)	35 (83.3)	
Yes	2 (3.8)	7 (16.7)	

Data are numbers of lesions, with percentages in parentheses. Categorical variables were compared by using the χ^2 test or Fisher exact test. †, data are medians, with interquartile ranges in parentheses and compared by using the Mann-Whitney *U* test.

Table 4 Comparison of quantitative parameters from preoperative spectral CT

Parameter	Ki-67 low expression (n=52)	Ki-67 high expression (n=42)	P value
Intratumoral NIC-AP†	0.16 (0.11, 0.21)	0.11 (0.08, 0.17)	0.017
Intratumoral NIC-PVP†	0.45 (0.39, 0.55)	0.37 (0.28, 0.47)	0.005
Peritumoral <1 cm NIC-AP†	0.05 (0.03, 0.08)	0.04 (0.02, 0.09)	0.221
Peritumoral <1 cm NIC-PVP‡	0.54±0.10	0.52±0.10	0.412
Transtumoral NIC-AP†	0.10 (0.06, 0.16)	0.08 (0.06, 0.13)	0.267
Transtumoral NIC-PVP†	0.50 (0.46, 0.57)	0.49 (0.40, 0.54)	0.188
λHU-AP†	3.63 (2.80, 5.71)	2.39 (1.73, 3.52)	0.001
λHU-PVP†	3.40 (2.72, 4.23)	2.45 (1.80, 3.47)	< 0.001
ECV†	0.29 (0.22, 0.37)	0.23 (0.19, 0.29)	0.001

†, data are medians, with interquartile ranges in parentheses and compared by using the Mann-Whitney *U* test; ‡, data are mean ± standard deviation and compared by using the two-sample *t*-test. AP, arterial phase; CT, computed tomography; ECV, extracellular volume; NIC, normalized iodine concentration; PVP, portal venous phase; λHU, slope of the spectral Hounsfield unit curve.

Table 5 Correlation between spectral CT parameters and the expression of Ki-67

Parameters	Correlation coefficient (r)	P value
Intratumoral NIC-AP	−0.248	0.016
Intratumoral NIC-PVP	−0.291	0.004
λHU-AP	−0.330	0.001
λHU-PVP	−0.367	<0.001
ECV	−0.339	0.001

AP, arterial phase; CT, computed tomography; ECV, extracellular volume; NIC, normalized iodine concentration; PVP, portal venous phase; λHU, slope of the spectral Hounsfield unit curve.

correlation between ECV derived from spectral CT and pathological immunohistochemistry in breast tumors, which also contradicts our findings. The ECV indicates that iodine more freely distributes in the plasma and extracellular space during measurement, with the tumor-to-aorta ratio representing the interstitial proportion (31). A previous study demonstrated an association between ECV and the degree of liver fibrosis (32). The accumulation of extracellular matrix is accompanied by an expansion of extracellular water, which serves as the distribution space for contrast agents. However, ECV can also be influenced by other factors. For example, hepatocyte swelling due to hepatic steatosis can compress the extracellular space and reduce ECV, whereas inflammation and venous congestion can induce edema, leading to an increase in ECV (33). To date, no studies have explored the potential of ECV to predict Ki-67 expression in HCC. Future research may focus on elucidating the impact of these confounding factors on liver ECV, thereby providing a more comprehensive understanding of its role in tumor biology.

In this study, the quantitative parameters of the peritumoral region were unable to differentiate between the high and low Ki-67 expression groups. Previous studies have shown that as liver fibrosis progresses, there is a reduction in liver parenchymal volume and microcirculatory changes, leading to increased hepatic resistance, reduced portal venous flow, and compensatory increases in hepatic arterial flow (34,35), all of which are correlated with the severity of fibrosis (36). Although no significant difference in the presence of cirrhosis was observed between the high and low Ki-67 expression groups in this study, the heterogeneity in fibrosis severity may have influenced the quantitative analysis of the peritumoral region. Currently, the quantitative analysis of the peritumoral region is predominantly conducted using radiomics. Studies have demonstrated that a 2-mm and a 5-mm peritumoral margin offer robust diagnostic performance for predicting microvascular invasion (MVI) in HCC and Ki-67 expression in breast cancer, respectively (37-39). However, manual delineation of ROIs poses challenges in achieving such precise margins and introduces inherent subjectivity, potentially impacting experimental outcomes. Future research should investigate the application of radiomics to further elucidate the relationship between peritumoral margins and Ki-67 expression in HCC.

In conclusion, multiple factors affect quantitative tumor analysis, including the tumor microenvironment, scanning techniques, and physiological changes linked to comorbidities. Further investigation is warranted to elucidate the specific mechanisms underlying these influences. Currently, no guidelines define the criteria for stratifying HCC patients into high and low Ki-67 expression groups. Therefore, large-scale, multicenter studies with more standardized protocols are necessary to further elucidate the relationship between quantitative spectral CT parameters and Ki-67 expression in HCC.

Conclusions

The qualitative and quantitative parameters derived from intratumoral spectral CT offer valuable insights for distinguishing between low and high Ki-67 expression in HCC.

Acknowledgments

None.

Footnote

Reporting Checklist: The authors have completed the STROBE reporting checklist. Available at https://qims.amegroups.com/article/view/10.21037/qims-24-2313/rc

Funding: This study was supported by the National Natural Science Foundation of China (No. 82060310).

Conflicts of Interest: All authors have completed the ICMJE uniform disclosure form (available at https://qims.amegroups.com/article/view/10.21037/qims-24-2313/coif).

The authors have no conflicts of interest to declare.

Ethical Statement: The authors are accountable for all aspects of the work in ensuring that questions related to the accuracy or integrity of any part of the work are appropriately investigated and resolved. This study was conducted in accordance with the Declaration of Helsinki and its subsequent amendments. This study was approved by the Medical Ethics Committee of the First Affiliated Hospital of Guangxi Medical University (approval No. 2024-E691-01). Written informed consent was provided by all patients prior to participation.

References

1. Bray F, Laversanne M, Sung H, Ferlay J, Siegel RL, Soerjomataram I, Jemal A. Global cancer statistics 2022: GLOBOCAN estimates of incidence and mortality worldwide for 36 cancers in 185 countries. CA Cancer J Clin 2024;74:229-63.
2. Zheng R, Zhang S, Zeng H, Wang S, Sun K, Chen R, Li L, Wei W, He J. Cancer incidence and mortality in China, 2016. J Natl Cancer Cent 2022;2:1-9.
3. Villanueva A. Hepatocellular carcinoma. N Engl J Med 2019;380:1450-62.
4. Yang JD, Hainaut P, Gores GJ, Amadou A, Plymoth A, Roberts LR. A global view of hepatocellular carcinoma: trends, risk, prevention and management. Nat Rev Gastroenterol Hepatol 2019;16:589-604.
5. Forner A, Reig M, Bruix J. Hepatocellular carcinoma. Lancet 2018;391:1301-14.
6. D'Errico A, Grigioni WF, Fiorentino M, Baccarini P, Grazi GL, Mancini AM. Overexpression of p53 protein and Ki67 proliferative index in hepatocellular carcinoma: an immunohistochemical study on 109 Italian patients. Pathol Int 1994;44:682-7.
7. Cao Y, Ke R, Wang S, Zhu X, Chen J, Huang C, Jiang Y, Lv L. DNA topoisomerase IIα and Ki67 are prognostic factors in patients with hepatocellular carcinoma. Oncol Lett 2017;13:4109-16.
8. Zhou J, Sun H, Wang Z, Cong W, Wang J, Zeng M, et al. Guidelines for the Diagnosis and Treatment of Hepatocellular Carcinoma (2019 Edition). Liver Cancer 2020;9:682-720.
9. Chen Y, Qin X, Long L, Zhang L, Huang Z, Jiang Z, Li C. Diagnostic Value of Gd-EOB-DTPA-Enhanced MRI for the Expression of Ki67 and Microvascular Density in Hepatocellular Carcinoma. J Magn Reson Imaging 2020;51:1755-63.
10. Majeed NF, Braschi Amirfarzan M, Wald C, Wortman JR. Spectral detector CT applications in advanced liver imaging. Br J Radiol 2021;94:20201290.
11. Cao X, Hu HG, Shen M, Deng K, Wu N. Correlation Between Quantitative Spectral CT Parameters and Ki-67 Expression in Lung Adenocarcinomas Manifesting as Ground-glass Nodules. Curr Med Imaging 2023;19:1052-62.
12. Lin L, Cheng J, Tang D, Zhang Y, Zhang F, Xu J, Jiang H, Wu H. The associations among quantitative spectral CT parameters, Ki-67 expression levels and EGFR mutation status in NSCLC. Sci Rep 2020;10:3436.
13. Wang X, Liu D, Zeng X, Jiang S, Li L, Yu T, Zhang J. Dual-energy CT quantitative parameters for evaluating Immunohistochemical biomarkers of invasive breast cancer. Cancer Imaging 2021;21:4.
14. Chen J, Tang L, Xie P, Qian T, Huang J, Liu K. Quantitative parameters of dual-layer spectral detector computed tomography for evaluating Ki-67 and human epidermal growth factor receptor 2 expression in colorectal adenocarcinoma. Quant Imaging Med Surg 2024;14:789-99.
15. Xu L, Yu Sun F, Xian Li G, Zai Yang L, Xiao Zhuo Y, Xiao Hu WXH, Wen X. Correlation between Spectral CT Parameters and Ki67 Expression in Hepatocellular Carcinoma. Curr Med Imaging 2023. [Epub ahead of print]. doi: 10.2174/0115734056227641231004042735.
16. Li C, Yue X, Chen S, Lin Y, Zhang Y, Liao L, Zhang P. Preoperative prediction of Ki-67 expression in hepatocellular carcinoma by spectral imaging on dual-energy computed tomography (DECT). Quant Imaging Med Surg 2024;14:8402-13.
17. Zhu XD, Zhang JB, Zhuang PY, Zhu HG, Zhang W, Xiong YQ, Wu WZ, Wang L, Tang ZY, Sun HC. High expression of macrophage colony-stimulating factor in peritumoral liver tissue is associated with poor survival

after curative resection of hepatocellular carcinoma. J Clin Oncol 2008;26:2707-16.
18. Zhao Y, Zhang J, Wang N, Xu Q, Liu Y, Liu J, Zhang Q, Zhang X, Chen A, Chen L, Sheng L, Song Q, Wang F, Guo Y, Liu A. Intratumoral and peritumoral radiomics based on contrast-enhanced MRI for preoperatively predicting treatment response of transarterial chemoembolization in hepatocellular carcinoma. BMC Cancer 2023;23:1026.
19. Wu C, Chen J, Fan Y, Zhao M, He X, Wei Y, Ge W, Liu Y. Nomogram Based on CT Radiomics Features Combined With Clinical Factors to Predict Ki-67 Expression in Hepatocellular Carcinoma. Front Oncol 2022;12:943942.
20. Kojima K, Takata A, Vadnais C, Otsuka M, Yoshikawa T, Akanuma M, Kondo Y, Kang YJ, Kishikawa T, Kato N, Xie Z, Zhang WJ, Yoshida H, Omata M, Nepveu A, Koike K. MicroRNA122 is a key regulator of α-fetoprotein expression and influences the aggressiveness of hepatocellular carcinoma. Nat Commun 2011;2:338.
21. Yang X, Ni H, Lu Z, Zhang J, Zhang Q, Ning S, Qi L, Xiang B. Mesenchymal circulating tumor cells and Ki67: their mutual correlation and prognostic implications in hepatocellular carcinoma. BMC Cancer 2023;23:10.
22. Wang P, Tang Z, Xiao Z, Wu L, Hong R, Duan F, Wang Y, Zhan Y. Dual-energy CT in predicting Ki-67 expression in laryngeal squamous cell carcinoma. Eur J Radiol 2021;140:109774.
23. Xie Y, Zhang S, Liu J, Liang X, Zhang X, Zhang Y, Zhang Z, Zhou J. Value of CT spectral imaging in the differential diagnosis of thymoma and mediastinal lymphoma. Br J Radiol 2019;92:20180598.
24. Chuang-Bo Y, Tai-Ping H, Hai-Feng D, Yong-Jun J, Xi-Rong Z, Guang-Ming M, Chenglong R, Jun W, Yong Y. Quantitative assessment of the degree of differentiation in colon cancer with dual-energy spectral CT. Abdom Radiol (NY) 2017;42:2591-6.
25. Sin SQ, Mohan CD, Goh RMW, You M, Nayak SC, Chen L, Sethi G, Rangappa KS, Wang L. Hypoxia signaling in hepatocellular carcinoma: Challenges and therapeutic opportunities. Cancer Metastasis Rev 2023;42:741-64.
26. Chen Z, Han F, Du Y, Shi H, Zhou W. Hypoxic microenvironment in cancer: molecular mechanisms and therapeutic interventions. Signal Transduct Target Ther 2023;8:70.
27. Jain RK. Normalization of tumor vasculature: an emerging concept in antiangiogenic therapy. Science 2005;307:58-62.
28. Grigioni WF, D'Errico A, Bacci F, Gaudio M, Mazziotti A, Gozzetti G, Mancini AM. Primary liver neoplasms: evaluation of proliferative index using MoAb Ki67. J Pathol 1989;158:23-9.
29. Murakami K, Kasajima A, Kawagishi N, Ohuchi N, Sasano H. Microvessel density in hepatocellular carcinoma: Prognostic significance and review of the previous published work. Hepatol Res 2015;45:1185-94.
30. Wang X, Du L, Cao Y, Chen H, Shi J, Zeng X, Lan X, Huang H, Jiang S, Lin M, Zhang J. Comparing extracellular volume fraction with apparent diffusion coefficient for the characterization of breast tumors. Eur J Radiol 2024;171:111268.
31. Chen Y, Shi K, Li Z, Wang H, Liu N, Zhan P, Liu X, Shang B, Hou P, Gao J, Lyu P. Survival prediction of hepatocellular carcinoma by measuring the extracellular volume fraction with single-phase contrast-enhanced dual-energy CT imaging. Front Oncol 2023;13:1199426.
32. Peng Y, Tang H, Huang Y, Yuan X, Wang X, Ran Z, Deng W, Liu R, Lan X, Shen H, Zhang J. CT-derived extracellular volume and liver volumetry can predict posthepatectomy liver failure in hepatocellular carcinoma. Insights Imaging 2023;14:145.
33. Bandula S, Punwani S, Rosenberg WM, Jalan R, Hall AR, Dhillon A, Moon JC, Taylor SA. Equilibrium contrast-enhanced CT imaging to evaluate hepatic fibrosis: initial validation by comparison with histopathologic sampling. Radiology 2015;275:136-43.
34. Richter S, Mücke I, Menger MD, Vollmar B. Impact of intrinsic blood flow regulation in cirrhosis: maintenance of hepatic arterial buffer response. Am J Physiol Gastrointest Liver Physiol 2000;279:G454-62.
35. Gülberg V, Haag K, Rössle M, Gerbes AL. Hepatic arterial buffer response in patients with advanced cirrhosis. Hepatology 2002;35:630-4.
36. Van Beers BE, Leconte I, Materne R, Smith AM, Jamart J, Horsmans Y. Hepatic perfusion parameters in chronic liver disease: dynamic CT measurements correlated with disease severity. AJR Am J Roentgenol 2001;176:667-73.
37. Kim TM, Lee JM, Yoon JH, Joo I, Park SJ, Jeon SK, Schmidt B, Martin S. Prediction of microvascular invasion of hepatocellular carcinoma: value of volumetric iodine quantification using preoperative dual-energy computed tomography. Cancer Imaging 2020;20:60.
38. Lu Y, Jin L, Ding N, Li M, Yin S, Ji Y. The value of multiparametric MRI radiomics and machine learning in predicting preoperative Ki-67 expression level in breast

cancer. BMC Med Imaging 2025;25:11.
39. Shang Y, Wang Y, Guo Y, Li S, Liao J, Hai M, Wang M, Tan H. The Clinical Study of Intratumoral and Peritumoral Radiomics Based on DCE-MRI for HER-2 Positive and Low Expression Prediction in Breast Cancer. Breast Cancer (Dove Med Press) 2024;16:957-72.

Cite this article as: Deng J, Tang Q, Wei Q, Ruan F, Li X, Long L. Preoperative assessment of Ki-67 expression in hepatocellular carcinoma using a multi-parametric spectral CT approach. Quant Imaging Med Surg 2025;15(5):4262-4273. doi: 10.21037/qims-24-2313